

Doping Metals

Deutsche Ausgabe: DOI: 10.1002/ange.201912293
Internationale Ausgabe: DOI: 10.1002/anie.201912293

Affecting an Ultra-High Work Function of Silver

Jin He, Jeff Armstrong, Peixi Cong, Barak Menagen, Lior Igaher, Andrew M. Beale, Lioz Etgar und David Avnir*

Abstract: An ultra-high increase in the WF of silver, from 4.26 to 7.42 eV, that is, an increase of up to circa 3.1 eV is reported. This is the highest WF increase on record for metals and is supported by recent computational studies which predict the potential ability to affect an increase of the WF of metals by more than 4 eV. We achieved the ultra-high increase by a new approach: Rather than using the common method of 2D adsorption of polar molecules layers on the metal surface, WF modifying components, L-cysteine and Zn(OH)₂, were incorporated within the metal, resulting in a 3D architecture. Detailed material characterization by a large array of analytical methods was carried out, the combination of which points to a WF enhancement mechanism which is based on directly affecting the charge transfer ability of the metal separately by cysteine and hydrolyzed zinc(II), and synergistically by the combination of the two through the known Zn-cysteine finger redox trap effect.

Introduction

The work function (WF) of a solid is the energy necessary to remove an electron originally at the Fermi level and place it at rest just outside the surface.^[1] This property affects major applications of metals which involve charge transport across their interfaces, including organic electronic devices, thermionic electron guns, sensing microelectronics and more.^[2–4] Methods for fine-tuning the WF in order to tailor it for the specific applications have been developed. The most common method used for modifying this property in metals has been the adsorption or covalent binding of polar molecules layers on the metal surface, thus creating an interfacial dipole barrier for the charge transport.^[5–7] Beyond fine-tuning, a long

standing challenge has been to increase the WF as high as possible, in order to further expand the range of possibilities of tailoring the desired WF value. Recent computational work predicted that the WF change of Ag or Au by a chemical modification can be as much as 4 eV and above.^[8,9] Yet, to the best of our knowledge, the highest experimental WF increase of a metal did not exceed 2 eV, as reported, for instance, by de Boer,^[5] Hofmann,^[10] and Frisbie.^[7]

Recently we have introduced an entirely new methodology for affecting the WF of metals, namely the doping of the metal with WF-modifying agents; that is, we move from derivatizing the 2D interface to the 3D volume of the metal. With this molecular doping we demonstrated the possibility to fine-tune the WF of gold and silver within the modest range of up to 1 eV.^[11] Being a new approach and following the above cited theoretical predictions, we set to explore the possibility to utilize the doping methodology in order to push the WF of silver into the ultra-high domain, which in the literature is defined as an increase of 2–3 eV.^[9–11] The materials methodology of molecular doping of metals employed herein involves a variety of reducing processes of metal cations in the presence of the molecule or nanoparticle (NP) to be entrapped (see refs. [12, 13] for reviews and [11, 14, 18] for recent examples). The resulting material is the metal in the form of tightly agglomerated nanometric crystals, incorporating the dopant molecule or NPs. The dopant is firmly held by the physical caging and by interactions between its functional moieties and the metallic surface of the nanocrystals that form the cages. It has been repeatedly shown, in previous applications studies of this materials methodology, that this 3D architecture is completely different from regular 2D adsorption, and various specific applications, such as in catalysis,^[17] biomaterials,^[15, 16] fuel cell,^[14] and more,^[18] are achieved only with the 3D entrapment. This is so because unlike 2D adsorption where the molecules interact with the metal typically through one moiety, in 3D entrapment the interaction between the dopant and the molecule is through all of its parts, therefore, the effect of the electrons ocean of the metal on the dopant and of the dopants orbitals on the metal, is different and significantly stronger.

We now report that the goal of pushing the WF of silver closer to the higher values predicted theoretically, was achieved: An ultrahigh increase in the WF of silver, from 4.26 to 7.42 eV, that is, an increase of up to about 3.1 eV (71.5 kcal mol^{−1}), was obtained, which is the highest on record for metals. The experimental approach has been a two-components doping of silver—L-cysteine and zinc hydroxide nanocrystals—each affecting the WF by the surface dipole formed at the interface, as well as by a mutual synergistic mechanism, all of which are detailed below. The effect is tunable, allowing

[*] Dr. J. He, B. Menagen, L. Igaher, Prof. Dr. L. Etgar, Prof. Dr. D. Avnir
Institute of Chemistry and The Center for Nanoscience and Nanotechnology, The Hebrew University of Jerusalem
Jerusalem 9190401 (Israel)
E-Mail: david.avnir@mail.huji.ac.il

Dr. J. Armstrong
ISIS Facility, Rutherford Appleton Laboratory
Harwell Oxford, Didcot, Oxfordshire OX11 0QX (UK)

P. Cong, Prof. Dr. A. M. Beale
Department of Chemistry, University College of London
Gordon Street, London WC1H 0AJ (UK)

and
Research Complex at Harwell, Rutherford Appleton Laboratory
Harwell Oxford, Didcot, Oxfordshire OX11 0FA (UK)

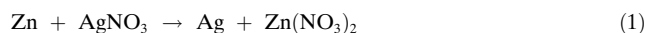
Supporting information and the ORCID identification number(s) for the author(s) of this article can be found under:
<https://doi.org/10.1002/anie.201912293>.

one to fine-tune the WF values of silver, over the wide range of 3.1 eV, as desired.

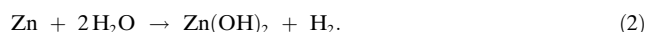
Results and Discussion

The chemistry of the entrapment:

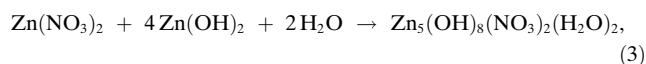
To achieve the dual-entrapment in silver and the two dopants, several processes and reactions between AgNO_3 , zinc, and L-cysteine, took place (see Experimental Details in the Supporting Information, and Scheme S1 in the Supporting Information). Equation (1) represents the formation of metallic silver atoms, which grow to nanocrystal nuclei of Ag, and which then grow further to the entrapping aggregated nanocrystals of metallic silver.



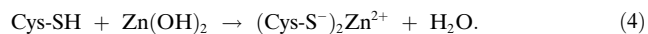
Zinc was selected as a reducing agent because it proved to be efficient in previous molecular doping of metals studies.^[17,19] Zinc nitrate is formed as a by-product, most of which is washed away, but some of which enters reaction (3) described below. A small excess of Zn is taken in order to produce also the oxidative hydrolysis product, Zn(OH)_2 , as a co-dopant according to



Under the reaction conditions, $\text{Zn(NO}_3)_2$ is not hydrolyzed to Zn(OH)_2 . Of the two reduction reactions, (1) and (2), the reduction by zinc of the silver cation (reduction potential of -0.76 V) is much faster than the reduction of water protons (0.0 V), and this difference leads to the ability to incorporate a small amount of Zn(OH)_2 nanocrystals within the forming silver matrix. $\text{Zn(NO}_3)_2$ reacts with Zn(OH)_2 forming zinc hydroxide nitrate:^[20]



but as we shall see below, the addition of cysteine, quenches this reaction, probably through the protective interaction of cysteine with Zn(OH)_2 .^[21]



The formation of the mercaptide $(\text{Cys-S}^-)_2\text{Zn}^{2+}$ is a key process in the biochemistry of Zn-metalloproteins,^[22] known as the „zinc-finger“,^[23,24] and of relevance to our report is its function as a powerful redox pair for electron trapping.^[25,26] The cysteine mercaptide of silver^[27] appears in the process as a transient gel, that does not interfere with the reduction process, because Zn is a strong enough reducing agent to operate on that silver compound as well.

An important interaction to be considered as well for the entrapment process and for the mechanism of the WF increase, is the well-known interaction of thiol groups with d-element metallic surfaces,^[28–30] occurring in our case between Cys-SH and both the metallic zinc and the formed metallic

silver.^[31] This interaction facilitates the homogeneous distribution of both dopants, and contributing to it are also the amino and the carboxylate groups which are good adsorptive anchors centers to a metal.^[32] At the used low concentrations of cysteine, it is not blocking the Zn from reducing the Ag^+ . Thus, while Gibbs free energy of metallic zinc-cysteine formation is -25 kJ mol^{-1} , the free energy of the reduction of Ag^+ by zinc is -308 kJ mol^{-1} .^[21]

What then are the reaction conditions which result in a doped metal? This question has been addressed in detail in previous studies of molecular entrapment within metals,^[16,17] where, in brief, the following mechanism has been suggested: Shortly after mixing the metal salt, the reducing agent and the dopants, reversible dopant–metal cation interactions occur (such as forming silver cysteinate), and the reducing agent is operating on both the free and the complexed cations. As a result, metallic atoms are formed, which begin to aggregate into metal nanocrystals, the elementary building blocks of the final doped metal. The dopant interacts reversibly with these forming crystallites, while more metal continues to form. If the condition, that the residence time of the adsorbed dopant is longer than the rate of reduction and formation of more metal is fulfilled, then precipitation/aggregation of the metal will capture the dopant in 3D metallic cages. In our case this condition is fulfilled, since, as mentioned above, cysteine strongly chemisorbs on metals, and this occurs during a fast reduction reaction. As the reduction—reaction (1)—proceeds, its rate slows down, and the slower hydrolysis—reaction (2)—becomes relatively more pronounced. At a later stage of the reduction reaction, the small excess of Zn has already shrunk to very small nanoparticles, accelerating the hydrolysis to Zn(OH)_2 nanoparticles (and also to Zn nanoparticles coated with Zn(OH)_2). We denote the hydrolysis product of metallic zinc as Zn^{II} and resulting doubly doped silver as $\text{cys/Zn}^{\text{II}}\text{@Ag}$.

The work function observations:

Table 1 displays the work functions and resistivities of $\text{cys/Zn}^{\text{II}}\text{@Ag}$ discs of various compositions, along with comparisons to pure Ag, $\text{Zn}^{\text{II}}\text{@Ag}$, and cys@Ag discs. The WF of the pure silver prepared by the same procedure but without the dopants is 4.26 eV; the WF of the dual doped silver is higher by more than 3 eV -7.42 eV—at a starting molar ratio of 0.1:0.6:1.0 cysteine:Zn:Ag. The 2D maps of one of the cys/

Tabelle 1: Work functions and resistivities for cysteine/ $\text{Zn}^{\text{II}}\text{@Ag}$ and reference samples.

Sample	Cysteine:Zn:Ag Starting molar ratio	WF [eV]	Resistivity [Ωcm]
1 Ag		4.26 ± 0.10	$3.0 \pm 0.2 \times 10^{-6}$
2 $\text{cys/Zn}^{\text{II}}\text{@Ag}$	0.10:0.60:1.00	7.42 ± 0.18	$4.8 \pm 0.3 \times 10^{-6}$
3 $\text{cys/Zn}^{\text{II}}\text{@Ag}$	0.10:0.55:1.00	6.50 ± 0.25	$4.5 \pm 0.3 \times 10^{-6}$
4 $\text{cys/Zn}^{\text{II}}\text{@Ag}$	0.10:0.52:1.00	5.76 ± 0.15	$4.1 \pm 0.4 \times 10^{-6}$
5 cys@Ag	0.10:1.00	5.05 ± 0.09	$3.9 \pm 0.2 \times 10^{-6}$
6 $\text{Zn}^{\text{II}}\text{@Ag}$	0.60:1.00	4.86 ± 0.15	$5.5 \pm 0.3 \times 10^{-5}$
7 $\text{Zn}^{\text{II}}\text{@Ag}$	1.00:1.00	5.06 ± 0.20	$3.2 \pm 0.3 \times 10^{-2}$



$\text{Zn}^{\text{II}}@\text{Ag}$ compositions and one of the blanks ($\text{cys}@\text{Ag}$) are shown in Figure 1, and reveal a homogenous distribution of this property on a 2×2 mm scale. Other compositions are shown in the Table 1, and it is remarkable that even 2 % mol doping of zinc increases the WF by 1.5 eV to 5.76 eV. Re-

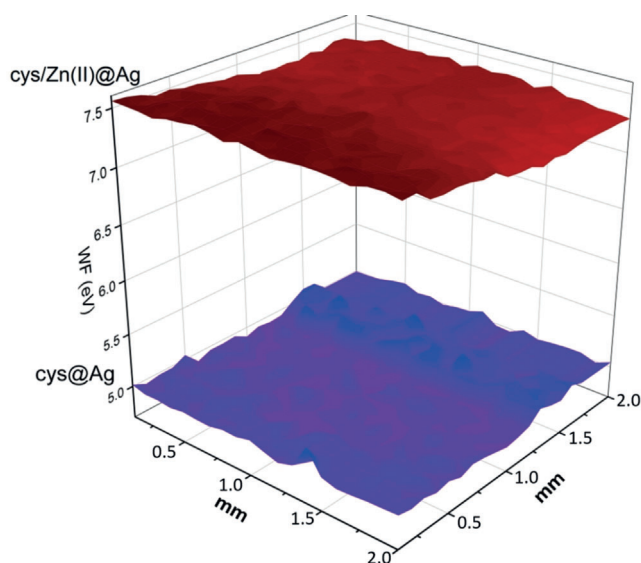


Figure 1. Work function 2D mapping of $\text{cys}/\text{Zn}^{\text{II}}@\text{Ag}$ at the maximal WF effect ratio (cysteine:Zn:Ag = 0.1:0.6:1.0, starting molar ratio), compared with the WF map of $\text{cys}@\text{Ag}$ for reference (cysteine:Zn:Ag = 0.1:0.5:1.0, starting molar ratio).

moving Zn all together, that is, having only cysteine doping, results in an increase to 5.05 eV, a value which is in agreement with the fine-tuning values of WF we reported for other organic molecules molecular doping of metals.^[8] Using only excess Zn (0.6:1, Zn:Ag) the WF value is again moderately changed to 5.36 ± 0.15 eV. Thus, combining the two dopants shows that there is strong synergism of action between them.

Several additional important observations were made: First, the conductivity of the doped discs remains high, only marginally smaller than that of the pure metal (Table 1); second, the WFs measured were stable for at least 3 months; and third, the high WF values are thermally stable, up to the decomposition temperature of cysteine (150°C), see TGA analysis below for details. Next, we move to a detailed characterization of the doped silver, which we use for a proposed mechanism of the WF strong enhancement.

Material characterization:

The composition for which the ultra-highest WF value -7.42 ± 0.18 eV (Table 1) was obtained, is at a molar ratio of cys:Zn:Ag of 0.10:0.10:1.00, (that is, an initial synthetic molar ratio of 0.10:0.60:1.00). The results of the XRD analysis for $\text{cys}/\text{Zn}^{\text{II}}@\text{Ag}$ prepared with increasing initial zinc amounts from 0.55 to 1 at a fixed cysteine/Ag molar ratio of 0.1:1 are shown in Figure 2 A. It is clearly seen, even with a molar Zn amount of 0.7 (40% excess for the reduction), that the do-

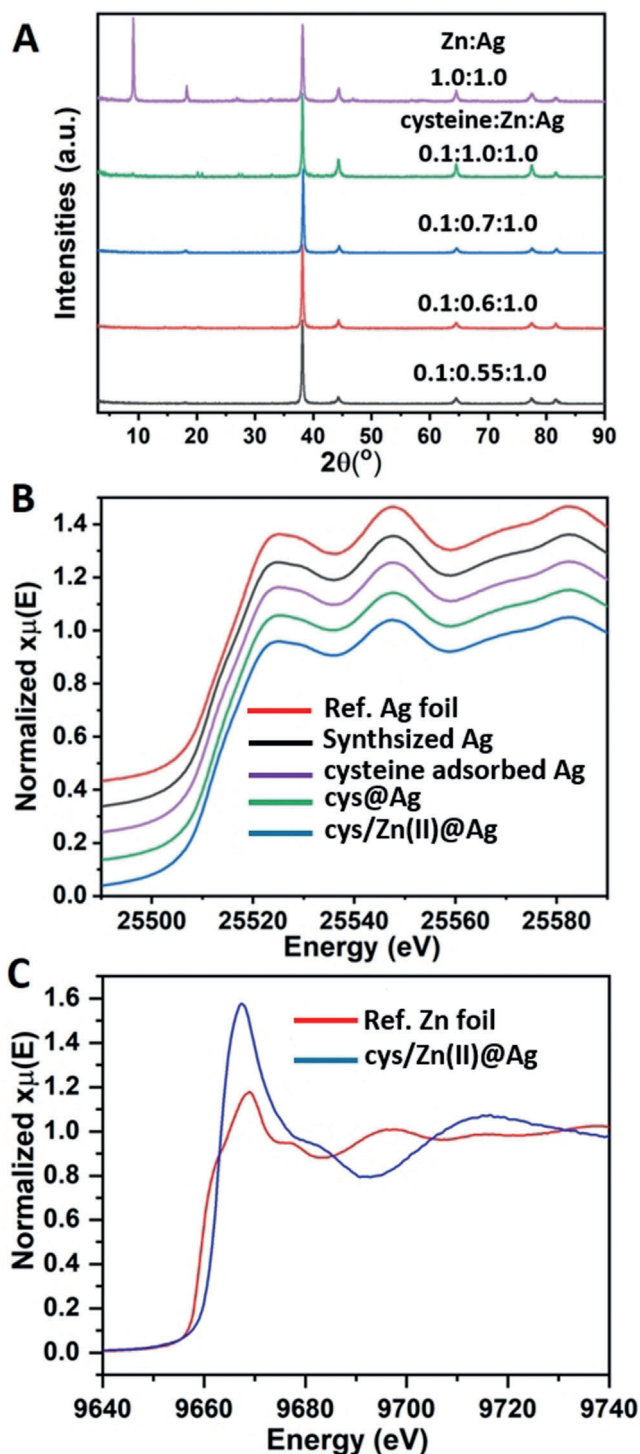


Figure 2. A) XRD patterns of $\text{cys}/\text{Zn}^{\text{II}}@\text{Ag}$ prepared with different molar ratios of zinc and comparison with the absence of cysteine (shown are the starting molar ratios). B) Normalized Ag K-edge XANES spectra of (from top to bottom) Ag metal foil, synthesized Ag powder, cysteine adsorbed on Ag, $\text{cys}@\text{Ag}$, and $\text{cys}/\text{Zn}^{\text{II}}@\text{Ag}$ (0.1:0.6:1.0, starting molar ratio). C) Normalized Zn K-edge XANES spectra of Zn metal foil and $\text{cys}/\text{Zn}^{\text{II}}@\text{Ag}$ (0.1:0.6:1.0, starting molar ratio).

minant peaks are of FCC metallic silver, appearing at $2\theta = 38.1, 44.4, 64.5, 77.4,$ and 81.6° which are associated with the (1

11), (2 00), (2 20), (3 11), and (2 22) crystallographic planes, respectively. Applying Scherrer's equation on the peaks of the XRD spectra indicate that the average size of the elementary nanocrystals building blocks is around 35 nm. This dominant pure silver phase indicates a quite uniform doping of the cysteine and of the excess Zn and it also indicates that the Zn^{II} particles are nanometric or even sub-nanometric particles. In fact, it is possible to see some $\text{Zn}(\text{OH})_2$ phase in Figure 2A only if a large excess of Zn — cys : Zn : Ag of 0.10:1.00:1.00 (starting molar ratio)—is taken (Figure 2A, green line). Interestingly, $\text{Zn}_5(\text{OH})_8(\text{NO}_3)_2(\text{H}_2\text{O})_2$ [Eq. (3)] is seen only if cysteine is removed (at $2\theta = 9.1$ and 18.1° ,^[33] Figure 2A, purple line), but only as a trace (Figure 2A, green line). This proves the binding of cysteine to $\text{Zn}(\text{OH})_2$, which is important for the mechanism of the WF increase given below.

X-ray absorption fine structure (XAFS) allows one to determine the chemical environment (valence states, coordination number) as well as the short-range structure around the silver and zinc atoms upon doping. The silver K-edge XAFS data is shown in Figure 2B, and in Figures S2, S3 and S4A in the Supporting Information. Both the X-ray absorption near-edge structure (XANES, Figure 2B) and the k^3 -weighted X-ray absorption fine structure spectra (EXAFS) (Supporting Information, Figure S2) closely match that of the bulk Ag (metal foil), indicating that all the Ag is in the metallic phase. This is also demonstrated by the Fourier transformed EXAFS (FT-EXAFS) shown in Figure S4A (Supporting Information). Furthermore, the FT-EXAFS spectra demonstrate a noticeable decrease in intensity of the Ag–Ag shell of the doped silver, which is expected when foreign species are incorporated. The spectra profiles of pure Ag and cysteine adsorbed on Ag are virtually identical, while a decrease in the Ag–Ag scattering intensity is observed in the spectra of the doped materials, $\text{cys}@Ag$ and $\text{cys}/\text{Zn}^{\text{II}}@Ag$, which again demonstrates the inherent difference between 2D adsorption and the 3D entrapment. This decrease is even more pronounced in $\text{cys}/\text{Zn}^{\text{II}}@Ag$, which indicates an enhanced co-doping effect on the silver. Evidence of Ag–S bond is seen in the Ag FT-EXAFS moduli of $\text{cys}@Ag$ and $\text{cys}/\text{Zn}^{\text{II}}@Ag$ (Detailed analysis appears in the Supporting Information, Figure S4A and Table S1). The Zn K-edge XANES spectra (Figure 2C) clearly show that the rise edge of $\text{cys}/\text{Zn}^{\text{II}}@Ag$ is 4.2 eV higher in energy compare to the reference metallic Zn foil which indicates that the 2+ oxidation state of Zn is the dominant species.^[34] The Zn FT-EXAFS spectra (Supporting Information, Figure S4B) reveal also that coordination environments are identical to Zn–O bond, which proves that the entrapped Zn is in the hydrolyzed form. The second shell scattering around 3.35 \AA in the Zn FT-EXAFS spectrum (Supporting Information, Figure S4B) reveals the scattering from a heavier atom, Ag, which indicates the existence of the $\text{Zn}(\text{OH})_2/\text{Ag}$ interface. This is relevant to the charge transfer between the two components as part of the mechanism of the WF increase (below). More XAFS analyses are provided and discussed in Figures S2, S3, S4 and Table S1 in the Supporting Information.

A typical high-resolution scanning electron microscopy (HR-SEM image) of the $\text{cys}/\text{Zn}^{\text{II}}@Ag$ composite (cysteine/ Zn/Ag = 0.1:0.6:1.0, the maximal WF increase composition,

Table 1) is displayed in Figure 3A. It is seen that the composite is made of hierarchically aggregated nanometric crystallites. This microstructure leads to a nitrogen-BET (Brunauer–Emmett–Teller) surface area of $6.21 \text{ m}^2 \text{ g}^{-1}$ displaying

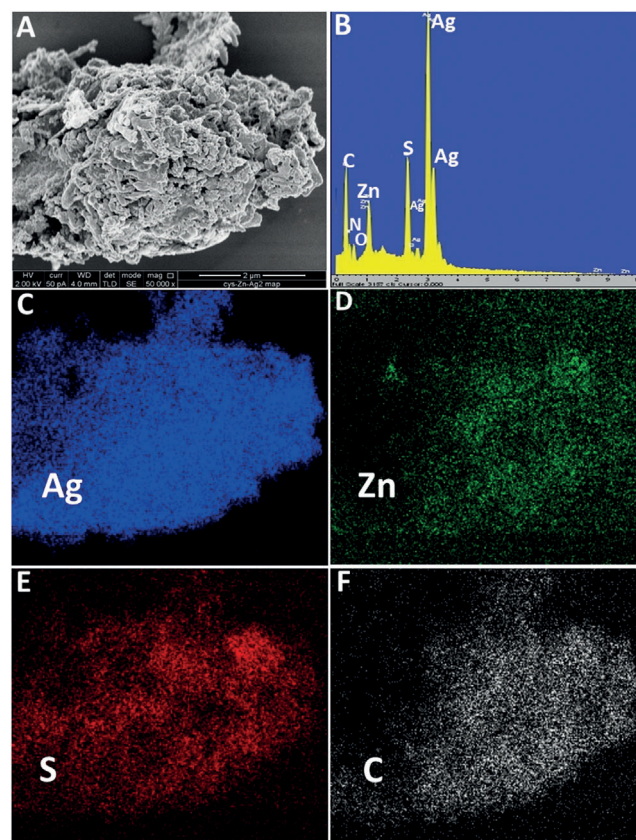


Figure 3. $\text{Cys}/\text{Zn}^{\text{II}}@Ag$ (0.1:0.6:1.0, starting molar ratios): A) SEM image, scale bar = $2 \mu\text{m}$. B) EDAX spectrum. EDS maps: C) Ag. D) Zn. E) S and F) C.

an adsorption-desorption isotherm typical of interstitial porosity (Supporting Information, Figure S5) with a Barrett–Joyner–Halenda (BJH) average mesopore diameter of 3.6 nm. After being pressed into disc for WF measurement, the mesoporous structure collapsed into almost non-porous materials (surface area $0.65 \text{ m}^2 \text{ g}^{-1}$). Coupling energy dispersive X-ray (EDAX) analysis (Figure 3B) with SEM imaging reveals the triple organic–inorganic hybrid nature of the composite with the appearance of silver, zinc, oxygen, carbon, nitrogen, and sulfur. Mapping of the elements (Figure 3C–F) demonstrates the homogeneous nature of the triple composite, at least on the scale of the diameter of the beam of electrons (ca. $1 \mu\text{m}$).

Thermogravimetric analysis (TGA) of $\text{cys}/\text{Zn}^{\text{II}}@Ag$ focuses on the organic component (cysteine), and it is compared in Figure 4A–D to pure cysteine and to $\text{cys}@Ag$ (without co-entrapped Zn). It is seen that the entrapment of cysteine, in either Ag or in $\text{Zn}^{\text{II}}@Ag$, affects a major lowering of the decomposition temperature (Figure 4A). The peak of cysteine at 210°C moves and splits into peaks at 165°C and 135°C , while retaining a small portion of the original 210°C peak



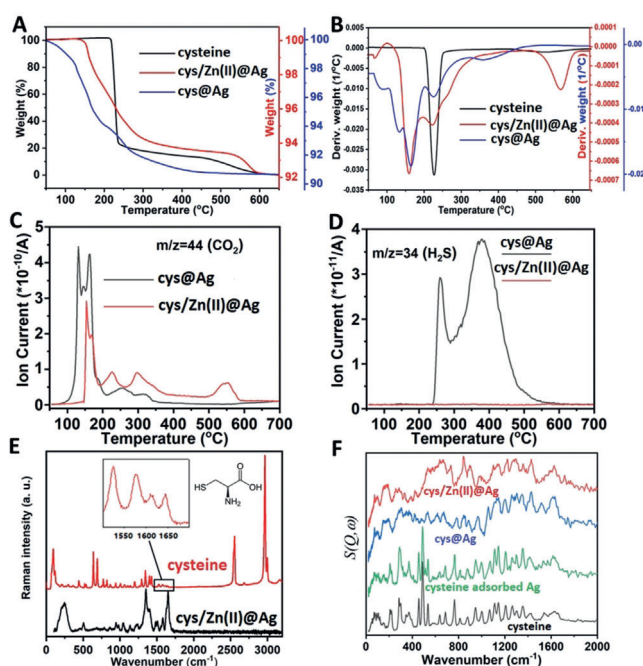


Figure 4. A) Thermogravimetric analysis (TGA) of the weight loss of cysteine(Zn^{II})@Ag (starting molar of 0.1:(0.6):1.0). B) The weight loss first derivative graphs and mass spectrometry coupled to TGA. C) $m/z = 44$ (CO_2). D) $m/z = 34$ (H_2S). E) Raman spectra of cysteine and $\text{cys}/\text{Zn}^{\text{II}}$ @Ag (0.1:0.6:1.0, starting molar ratio). F) INS spectra of (from top to bottom) $\text{cys}/\text{Zn}^{\text{II}}$ @Ag (0.1:0.6:1.0, starting molar ratio), $\text{cys}@Ag$, cysteine adsorbed on Ag, and cysteine.

(Figure 4B). This very significant lowering reflects the known catalytic effect of silver on thermal degradation, which has been observed previously in other organically doped silver^[35,36] and is a direct proof of the entrapment of cysteine. The broadening of the peaks in the doped form is a reflection of a more heterogeneous environment that the dopant molecules experience, that is, of the various cage and pore geometries where the dopant molecules reside. The main gaseous products of the thermal decomposition of pure cysteine are H_2S and CO_2 , obtained by the cleavage of C–C and C–S bonds,^[37] are shown in Figure 4C,D. Interestingly, the presence of Zn^{II} strongly influences the decomposition behavior of cysteine compared with entrapment in pure silver, indicating a strong interaction between them. Firstly, the catalytic effect of silver has been attenuated in presence of zinc, as the decomposition of cysteine occurs at higher temperature; and second, there appears a peak at the elevated temperature of 550°C (Figure 4A), which is associated with CO_2 , as shown by the MS-coupled to the TGA of $\text{cys}/\text{Zn}^{\text{II}}$ @Ag (Figure 4C). The absence of an H_2S signal during the calcination (Figure 4D) points to the probable forming of ZnS upon thermolysis. As the enthalpy of formation ($\Delta_f H_{298}^\theta$) of ZnS ($-204.6 \text{ kJ mol}^{-1}$) is much lower than that of AgS ($-32.59 \text{ kJ mol}^{-1}$), the formation of the thermally stable ZnS is preferred. Compared to the decomposition of cysteine (ca. 20 wt. % of composites), the weight loss of Zn^{II} dehydration ($< 2 \text{ wt. \%}$) is negligible. The strong cysteine–Zn interaction revealed by the TGA analysis is an important element of the WF-increase mechanism detailed in the next section.

This TGA analysis correlates well with the WF thermal stability of $\text{cys}/\text{Zn}^{\text{II}}$ @Ag (Supporting Information, Figure S6): It is seen that the ultrahigh WF is maintained up to 150°C and decreases significantly with further heating to 200°C and 300°C , at which the thermal decomposition of cysteine occurs according to the TGA analysis. The importance of this heating experiment is that it proves the necessary role of cysteine in the WF increase, because that increase is stable up to the point where this amino acid decomposes (150°C).

To additionally explore the specific interactions of cysteine with the solid components Raman spectroscopy has been carried out. The two enhanced Raman bands in the $1500\text{--}1700 \text{ cm}^{-1}$ (inset of Figure 4E) are in agreement with the reported Raman spectrum of the mercaptide $\text{Zn}(\text{cys})_2$ ^[38] (Supporting Information, Figure S9) which is formed in reaction (4) above. $\text{Zn}(\text{cys})_2$ is a component of the redox controlling „zinc-finger effect“,^[25,26,39] which contributes to the WF large increase. Indeed, in this context it is noteworthy to point out that the small peak at ca. 504 cm^{-1} is associated with an S–S dipeptide bond pointing to the existence of cystine (the oxidized dimer of cysteine), which again is relevant to the zinc-finger phenomenon discussed below. Notably, Shkirskiy et al.^[21] reported that in the Zn oxide-hydroxide film/cysteine system, the value of the Gibbs free energy of the complex formation between these two components is -100 kJ mol^{-1} , that is, the formation of $\text{Zn}(\text{cys})_2$ is thermodynamically favored over simple adsorption, for which, G^0 was about -25 kJ mol^{-1} . Last but not least, inelastic neutron scattering spectroscopy (INS) is also well suited to the study of the interaction of a metal with molecules, because the metal cages are essentially invisible to neutrons and the hydrogen rich organic molecules are strong scatterers.^[40,41] As shown in Figure 4F, adsorption and entrapment are completely different: In the adsorbed case, the molecule spectrum is very similar to that of pure cysteine with only minor difference, while major differences are observed in the entrapment case. It is noticeable that the disappearance of S–H in-plane bend and significant attenuation of the NH_3 rock only occurs in $\text{cys}/\text{Zn}^{\text{II}}$ @Ag, which points to the formation of Zn-cysteine complex. More Raman and INS analyses can be found in the Supporting Information (Figure S7–S10).

Proposed origin of the ultra-high work function and conclusion:

Based on the detailed multi-analytical investigations of the structure and properties of the various doped silver samples, we propose that the large increase in the work function is due to the combined effect of these components (Figure 5): Cysteine, Zn^{II} and $\text{Zn}(\text{cys})_2$. Cysteine is a well-known corrosion resisting agent, the action of which has been attributed to the interaction of the thiol group with the metal surface.^[28,29,42] The adsorption of the thiol group creates a dipole barrier for charge transfer from the metal (Figure 5B), affecting an increase in the WF of the protected metal of the order of 1 eV (Table 1).^[6,7,43] Likewise the contribution from Zn^{II} is attributed to the well-documented surface dipole due to charge transfer at a metal-insulator interface (Figure 5B),^[44–46] where common insulators have been metal

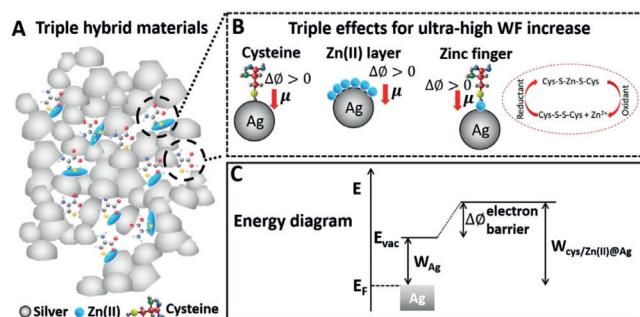


Figure 5. The proposed mechanism of the ultrahigh work function effect. A) The general structure of the doped silver. B) The origin of the ultra-high increase in the WF. The surface dipole/charge transfer is affected by three components: The interfaces of cysteine/Ag (left) and of $Zn(OH)_2/Ag$ (center) and the cysteine– Zn^{2+} („zinc-finger“)/Ag interface (right). C) The energy diagram: The increase in the WF is due to the electron barrier, keeping the Fermi level of Ag unaffected.

oxides.^[47–49] In this case, the suggested mechanism in the literature has been the decay of the metal wave function into the insulator where the metal conduction band overlaps with the insulator band gap. For instance, increases of the order of 0.5–1 eV have been observed with titania and silica.^[49] Indeed, we observed increases of 0.1–1.0 eV when silver was doped with zinc but without cysteine (Table 1). The second shell scattering of Zn EXAFS and the XRD, indicate that the extremely small Zn^{II} is homogeneously distributed and this facilitates the efficient formation of a metal-dielectric interface between Zn^{II} and the silver matrix. The metal-insulator distance is also a key aspect in determining the work function change. Pacchioni et al.^[49] showed that efficient WF changes occur at a distance range of 0.72–2.73 Å. In the $cys/Zn^{II}@Ag$, the Ag–O distance at Zn^{II}/Ag interface can be estimated to be about 1.66 Å (Figure S4C, detailed estimation has been discussed in Supporting Information), which is therefore supposed to be an appropriate range for efficient charge transfer.

The third contributor to the WF increase is the combination of the two dopants, cysteine and Zn^{II} , namely the mercaptide $Zn(cys)_2$ [Eq. (4)], which is a component of the cysteine– Zn^{2+} („zinc-finger“) electron-trap redox mechanism. This mechanism, commonly found in biochemical systems, acts as a powerful anti-oxidation agent by shuttling electrons back and forth between two Zn/cysteine species,^[25,26,39] (Figure 5 B). Thus, $cys-S-Zn-S-cys$ contributes to the blocking of the ability of the metal electron to leave it (increase in WF) by acting as an electron releasing source, while the second component of the zinc finger, the $cys-S-S-cys/Zn^{2+}$ pair, can act as an electron trap for an injected electron. Both $Zn(cys)_2$ and cystine were indeed detected, as described above. Also supporting our observations and conclusions are the computational studies cited in the Introduction, where an ultrahigh WF increase (ca. 4 eV) of silver has been predicted in a triple organic–silicone–silver system,^[9] quite close to the ultrahigh WF increase (> 3 eV) we achieved in our system. We also note that recent investigations reveal that the WF alternation by chemical modification is highly dependent on the molecules orientation (bending and rotation of substituents)^[8,10,50] at the metal–dielectric interface.

And indeed, as revealed by the INS spectra, the molecular state of cysteine in the entrapped case has been changed significantly.

Conclusion

Herein, we report on affecting an ultrahigh WF of silver, reaching a value of 7.42 eV, which, to the best of our knowledge is the highest recorded for a metal by a chemical modification, and agrees with computational predictions. The approach is new, and involves 3D doping of the bulk of the metal, rather than the common 2D surface treatment. Co-doping with the L-cysteine and hydrolyzed zinc (II) leads to contributions to the increase in the WF by each component separately by affecting directly the charge transfer ability of the metal, and synergistically by the combination of the two components through the known Zn–Cys finger effect. The ability to tailor WF changes from the standard value of silver and up over a wide range, will certainly find its applications wherever tuning of the WF is needed for the design of charge transport devices. For example, silver has been applied as a hole-extraction material in inverted polymer solar cells (IPSCs) owing to its electronic properties and its work function. In an IPSC, the WF should be sufficiently high to allow for the build-up of the electric field within the active component in the cell to maximize the extraction of holes from the active material.^[9,51]

Acknowledgements

Supported by the Ministry of Science, Technology & Space of Israel through grant No. 3-12948. The authors acknowledge the Diamond Light Source, UK (project no. SP18835, B18 beamline) and the ISIS facility, UK (project no. 1720114, TOSCA spectrometer) for the provision of beamtime. J.H. and B.M. acknowledge Newton Funding for supporting to use the ISIS facility. We thank Mr. Giannantonio Cibin for assistance in performing the XAFS measurements.

Conflict of interest

The authors declare no conflict of interest.

Stichwörter: Metalletotierung · Kelvin-Sonde · Redoxfallen-Effekt · Silber · Austrittsarbeit

- [1] N. D. Lang, W. Kohn, *Phys. Rev. B* **1971**, 3, 1215.
- [2] I. H. Campbell, S. Rubin, T. A. Zawodzinski, J. D. Kress, R. L. Martin, D. L. Smith, N. N. Barashkov, J. P. Ferraris, *Phys. Rev. B* **1996**, 54, R14321.
- [3] H. Zhang, J. Tang, Q. Zhang, G. Zhao, G. Yang, J. Zhang, O. Zhou, L. Qin, *Adv. Mater.* **2006**, 18, 87–91.



- [4] J. P. Barnak, R. S. Chau, C. Liang, US Patent US7022559B2, **2006**.
- [5] B. de Boer, A. Hadipour, M. M. Mandoc, T. van Woudenberg, P. W. M. Blom, *Adv. Mater.* **2005**, *17*, 621–625.
- [6] M. L. Sushko, A. L. Shluger, *Adv. Mater.* **2009**, *21*, 1111–1114.
- [7] V. B. Engelkes, J. M. Beebe, C. D. Frisbie, *J. Am. Chem. Soc.* **2004**, *126*, 14287–14296.
- [8] O. T. Hofmann, D. A. Egger, E. Zojer, *Nano Lett.* **2010**, *10*, 4369–4374.
- [9] P. D. Taylor, D. A. Osborne, S. A. Tawfik, T. Morishita, M. J. S. Spencer, *Phys. Chem. Chem. Phys.* **2019**, *21*, 7165–7173.
- [10] O. T. Hofmann, H. Glowatzki, C. Bürker, G. M. Rangger, B. Bürker, J. Niederhausen, T. Hosokai, I. Salzmänn, R.-P. Blum, R. Rieger, *J. Phys. Chem. C* **2017**, *121*, 24657–24668.
- [11] J. He, L. Iagher, L. Etgar, D. Avnir, *Chem. Commun.* **2018**, *54*, 7203–7206.
- [12] D. Avnir, *Adv. Mater.* **2018**, *30*, 1706804.
- [13] D. Avnir, *Acc. Chem. Res.* **2014**, *47*, 579–592.
- [14] N. Ralbag, M. Mann-Lahav, E. S. Davydova, U. Ash, R. Galed, M. Handl, R. Hiesgen, E. Magliocca, W. Mustain, J. He, P. Cong, A. M. Beale, G. S. Grader, D. Avnir, D. R. Dekel, *Matter* **2019**, *1*, 959–975.
- [15] T. S. Bauer, B. Menagen, D. Avnir, Z. Hayouka, *Sci. Rep.* **2019**, *9*, 1–8.
- [16] B. Menagen, D. Avnir, *ACS Biomater. Sci. Eng.* **2019**, *5*, 2355–2364.
- [17] L. Shapero, D. Avnir, *ChemCatChem* **2017**, *9*, 816–823.
- [18] N. Ralbag, I. Felner, D. Avnir, *Phys. Rev. B* **2019**, *99*, 64411.
- [19] R. Ben-Knaz, D. Avnir, *Biomaterials* **2009**, *30*, 1263–1267.
- [20] P. Li, Z. P. Xu, M. A. Hampton, D. T. Vu, L. Huang, V. Rudolph, A. V. Nguyen, *J. Phys. Chem. C* **2012**, *116*, 10325–10332.
- [21] V. Shkirskiy, P. Keil, H. Hintze-Bruening, F. Leroux, F. Brisset, K. Ogle, P. Volovitch, *Corros. Sci.* **2015**, *100*, 101–112.
- [22] N. Pace, E. Weerapana, *Biomolecules* **2014**, *4*, 419–434.
- [23] F. D. Urnov, J. C. Miller, Y.-L. Lee, C. M. Beausejour, J. M. Rock, S. Augustus, A. C. Jamieson, M. H. Porteus, P. D. Gregory, M. C. Holmes, *Nature* **2005**, *435*, 646.
- [24] M. Bibikova, K. Beumer, J. K. Trautman, D. Carroll, *Science* **2003**, *300*, 764.
- [25] W. Maret, *Antioxid. Redox Signaling* **2006**, *8*, 1419–1441.
- [26] K.-D. Kröncke, L.-O. Klotz, *Antioxid. Redox Signaling* **2009**, *11*, 1015–1027.
- [27] B. O. Leung, F. Jalilehvand, V. Mah, M. Parvez, Q. Wu, *Inorg. Chem.* **2013**, *52*, 4593–4602.
- [28] N. H. Helal, W. A. Badawy, *Electrochim. Acta* **2011**, *56*, 6581–6587.
- [29] M. B. Radovanović, M. B. Petrović, A. T. Simonović, S. M. Milić, M. M. Antonijević, *Environ. Sci. Pollut. Res.* **2013**, *20*, 4370–4381.
- [30] D. Kesavan, M. Gopiraman, N. Sulochana, *Chem. Sci. Rev. Lett.* **2012**, *1*, 1–8.
- [31] S. Fischer, A. C. Papageorgiou, M. Marschall, J. Reichert, K. Diller, F. Klappenberger, F. Allegretti, A. Nefedov, C. Wöll, J. V. Barth, *J. Phys. Chem. C* **2012**, *116*, 20356–20362.
- [32] Q. Chen, N. V. Richardson, *Nat. Mater.* **2003**, *2*, 324.
- [33] T. N. Ramesh, T. L. Madhu, *Int. J. Inorg. Chem.* **2015**, *0*, 536470.
- [34] A. K. Yadav, S. M. Haque, S. Tripathi, D. Shukla, M. A. Ahmed, D. M. Phase, S. Bandyopadhyay, S. N. Jha, D. Bhattacharyya, *RSC Adv.* **2016**, *6*, 74982–74990.
- [35] H. Behar-Levy, G. E. Shter, G. S. Grader, D. Avnir, *Chem. Mater.* **2004**, *16*, 3197–3202.
- [36] G. Neshet, M. Aylien, G. Sandaki, D. Avnir, G. Marom, *Adv. Funct. Mater.* **2009**, *19*, 1293–1298.
- [37] V. A. Yablokov, Y. A. Vasina, I. A. Zelyaev, S. V. Mitrofanova, *Russ. J. Gen. Chem.* **2009**, *79*, 1141.
- [38] S. Foley, M. Enescu, *Vib. Spectrosc.* **2007**, *44*, 256–265.
- [39] X. Wu, N. H. Bishopric, D. J. Discher, B. J. Murphy, K. A. Webster, *Mol. Cell. Biol.* **1996**, *16*, 1035–1046.
- [40] S. F. Parker, A. J. Ramirez-Cuesta, L. Daemen, *Spectrochim. Acta Part A* **2018**, *190*, 518–523.
- [41] S. F. Parker, F. Fernandez-Alonso, A. J. Ramirez-Cuesta, J. Tomkinson, S. Rudic, R. S. Pinna, G. Gorini, J. Fernández Castañón, *J. Phys. Conf. Ser.* **2014**, *554*, 012003.
- [42] K. M. Ismail, *Electrochim. Acta* **2007**, *52*, 7811–7819.
- [43] R. W. Zehner, B. F. Parsons, R. P. Hsung, L. R. Sita, *Langmuir* **1999**, *15*, 1121–1127.
- [44] S. Prada, U. Martinez, G. Pacchioni, *Phys. Rev. B* **2008**, *78*, 235423.
- [45] S. Choi, D.-H. Lee, S. G. Louie, J. Clarke, *Phys. Rev. Lett.* **2009**, *103*, 197001.
- [46] C. Cen, S. Thiel, G. Hammerl, C. W. Schneider, K. E. Andersen, C. S. Hellberg, J. Mannhart, J. Levy, *Nat. Mater.* **2008**, *7*, 298.
- [47] M. Sterrer, T. Risse, U. M. Pozzoni, L. Giordano, M. Heyde, H.-P. Rust, G. Pacchioni, H.-J. Freund, *Phys. Rev. Lett.* **2007**, *98*, 96107.
- [48] S. Lu, Z. Qin, Q. Guo, G. Cao, *Appl. Surf. Sci.* **2017**, *392*, 849–853.
- [49] L. Giordano, F. Cinquini, G. Pacchioni, *Phys. Rev. B* **2006**, *73*, 45414.
- [50] E. Zojer, T. C. Taucher, O. T. Hofmann, *Adv. Mater. Interfaces* **2019**, *6*, 1900581.
- [51] C. Hu, D. Liu, Y. Xiao, L. Dai, *Prog. Nat. Sci. Mater. Int.* **2018**, *28*, 121–132.

Manuskript erhalten: 25. September 2019

Veränderte Fassung erhalten: 21. November 2019






Akzeptierte Fassung online: 10. Januar 2020

Endgültige Fassung online: ■ ■ ■ ■ ■ ■ ■ ■ ■ ■

Forschungsartikel

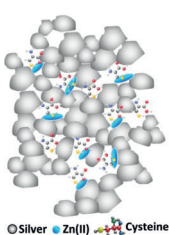


Metalldotierung

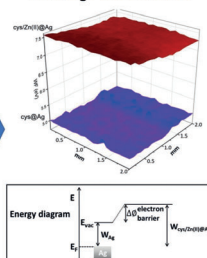
J. He, J. Armstrong, P. Cong, B. Menagen,
L. Igaher, A. M. Beale, L. Etgar,
D. Avnir*     

Affecting an Ultra-High Work Function of
Silver

Triple Hybrid Materials:
Cysteine/Zn(OH)₂@Ag



Ultra-High Work Function



Eine ultrahohe Steigerung der Austrittsarbeit (WF) von Silber von 4.26 auf 7.42 eV wird beim dualen Einschluss der WF-modifizierenden Komponenten L-Cystein und Zn(OH)₂ in das Metall beobachtet. Diese Verstärkung basiert auf der direkten Beeinflussung der Ladungstransferfähigkeit des Metalls – zum einen separat durch Cystein und hydrolysiertes Zink(II), zum anderen synergistisch durch die Kombination der beiden durch den Zn-Cysteinfinger-Redoxfallen-Effekt.